RNA (2001), *7*:887–895. Cambridge University Press. Printed in the USA.

Imaging of single hairpin ribozymes in solution by atomic force microscopy

MICHAEL J. FAY,[1] NILS G. WALTER,[2] and JOHN M. BURKE[1]

[1]Markey Center for Molecular Genetics, Department of Microbiology and Molecular Genetics, The University of Vermont, Burlington, Vermont 05405, USA

ABSTRACT

The hairpin ribozyme is a short endonucleolytic RNA motif isolated from a family of related plant virus satellite RNAs. It consists of two independently folding domains, each comprising two Watson–Crick helices flanking a conserved internal loop. The domains need to physically interact (dock) for catalysis of site-specific cleavage and ligation reactions. Using tapping-mode atomic force microscopy in aqueous buffer solution, we were able to produce high quality images of individual hairpin ribozyme molecules with extended terminal helices. Three RNA constructs with either the essential cleavage site guanosine or a detrimental adenosine substitution and with or without a 6-nt insertion to confer flexibility to the interdomain hinge show structural differences that correlate with their ability to form the active docked conformation. The observed contour lengths and shapes are consistent with previous bulk-solution measurements of the transient electric dichroism decays for the same RNA constructs. The active docked construct appears as an asymmetrically docked conformation that might be an indication of a more complicated docking event than a simple collapse around the interdomain hinge.

Keywords: AFM; catalytic RNA; conformational change; domain docking; nickel(II); RNA cleavage; RNA structure; SFM

INTRODUCTION

The hairpin ribozyme is a 50-nt-long catalytic RNA motif, derived from the satellite RNAs of tobacco ringspot and related plant viruses (Buzayan et al., 1986; Hampel & Tritz, 1989; Walter & Burke, 1998). This site-specific RNA endonuclease generates 5′ and 3′ cleavage products with 2′-3′ cyclic phosphate and 5′ hydroxyl termini, respectively. The minimal *trans*-cleaving ribozyme–substrate complex consists of two independently folding domains: domain A, consisting of the substrate and the substrate-binding strand, and the catalytically essential domain B. Each domain is comprised of a highly conserved internal loop flanked by two standard Watson–Crick helices (for review, see Walter & Burke, 1998).

The existence of a functionally important interaction between the domains has been established previously by linker-insertion studies (Feldstein & Bruening, 1993; Komatsu et al., 1996; Walter & Burke, 1998) and reconstitution experiments (Butcher et al., 1995). However, our knowledge of the reaction pathway is limited. Recently, folding from an extended (open) into a docked (closed) conformation has been identified as an essential step that precedes catalysis (Hampel et al., 1998; Walter et al., 1998, 1999). A single mutation of a cleavage site nucleotide, G + 1, can prevent this folding transition and suppress cleavage due to the loss of an essential long-range Watson–Crick interaction with a cytosine in domain B (Pinard et al., 1999; Fig. 1B).

In recent years, atomic force microscopy (AFM; also scanning force microscopy, SFM) has developed into a powerful tool for imaging individual biological molecules in aqueous buffers, under conditions where the molecule retains activity (for review, see Hansma & Hoh, 1994; Lindsay, 1994; Yang & Shao, 1995; Bustamante et al., 1997; Fritz et al., 1997; Hansma et al., 1997; Miles, 1997; Hansma & Pietrasanta, 1998; Heinz & Hoh, 1999; Engel et al., 1999). The most widely used method, tapping-mode AFM, obtains data by gently tapping a sharply pointed probe attached to a flexible cantilever in a raster scan over a surface, recording the height deflections of the probe. The collected data can

Reprint requests to: John M. Burke, Markey Center for Molecular Genetics, Department of Microbiology and Molecular Genetics, The University of Vermont, Burlington, Vermont 05405, USA; email: John.Burke@uvm.edu; or Nils G. Walter, Department of Chemistry, The University of Michigan, Ann Arbor, Michigan 48109-1055, USA; email: nwalter@umich.edu.

[2]Present address: Department of Chemistry, The University of Michigan, Ann Arbor, Michigan 48109-1055, USA.

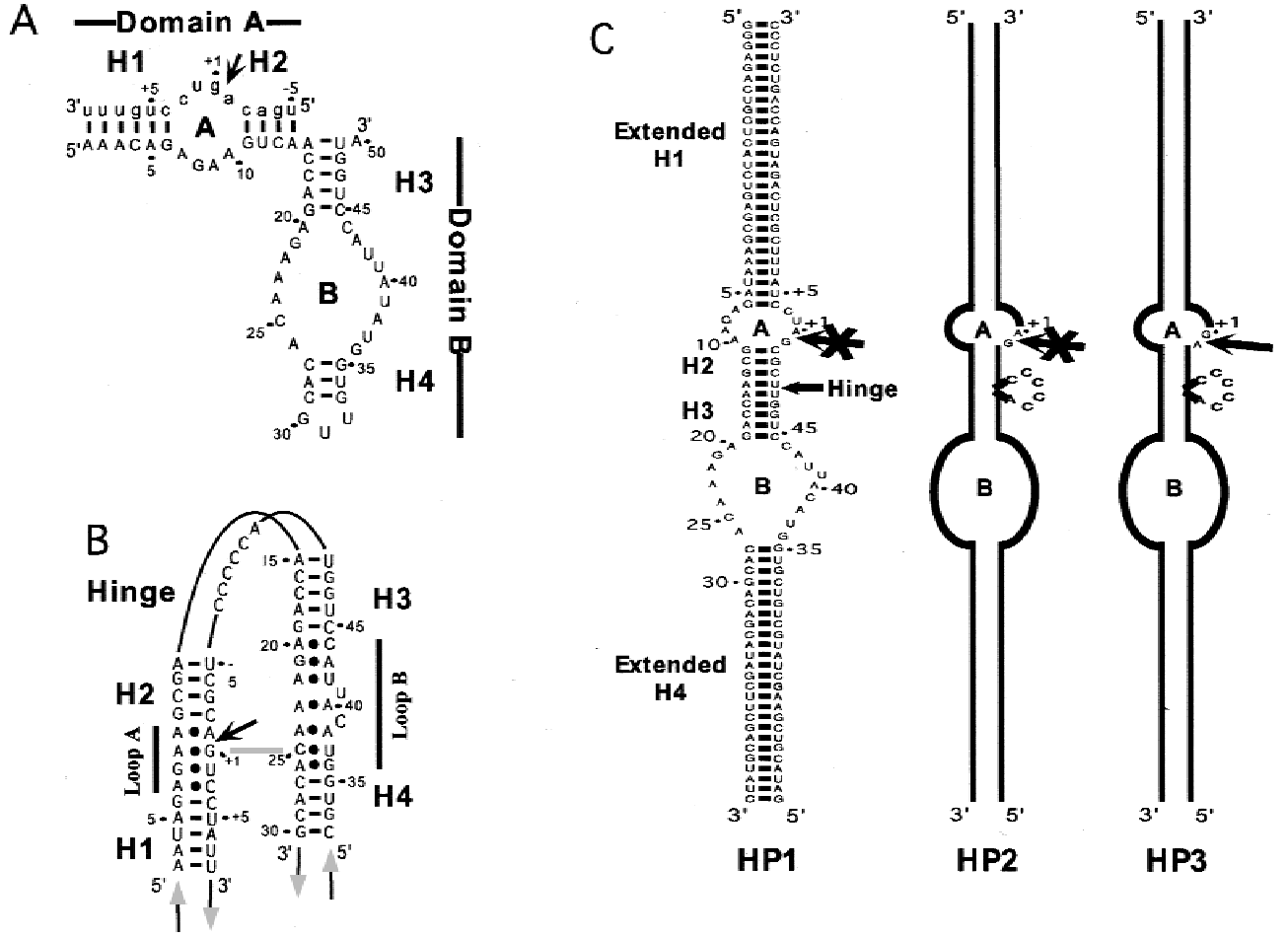

FIGURE 1. Structure of the hairpin ribozyme. **A**: Primary and secondary structure of the naturally occurring hairpin ribozyme from the negative strand of the tobacco ringspot virus satellite RNA. The two independently folding domains A and B each consist of two helices H1, H2 and H3, H4 (black lines: Watson–Crick base pairs) that flank the internal loops A and B, respectively. Ribozyme nucleotides are numbered 1 through 50. The external substrate (lower case letters, nucleotides numbered −5 through +9) is bound in domain A. Arrow: cleavage site. **B**: Current model of the interaction between the two domains, including a crucial Watson–Crick base pair between the +1 substrate and 25 ribozyme positions (Pinard et al., 1999). Non Watson–Crick base pairs with internal loops are indicated by a solid dot and are as described (Cai & Tinoco, 1996; Butcher et al., 1999). **C**: The three ribozyme-derived constructs employed in this AFM study. Helices 1 and 4 are extended, and the substrate strand (with the cleavage site arrow) is linked to the 3′ ribozyme segment either directly (HP1) or through a 6-nt linker bulge (HP2 and HP3). Sequence changes around the cleavage site either produce a catalytically active (arrow) or inactive (crossed-out arrow) construct. All three constructs share the same 5′ ribozyme segment.

be used to compose a contour plot of the scanned area that may, for example, consist of nucleic acid molecules bound to an atomically flat, freshly cleaved muscovite mica surface. The major advantage of this technology is the ability to observe a single molecule at a time, rather than an entire population. In this way, information about the population can be compiled by examining each molecule individually, as part of the population. The sample preparation method and buffer composition are each critical for successful imaging by AFM (Hansma & Laney, 1996).

To date, RNA molecules that have been visualized by AFM are relatively large, such as viral double-stranded RNA (dsRNA) (Lyubchenko et al., 1992; Drygin et al., 1998) or nascent RNA from an active transcription complex, usually bound to protein or imaged in air after drying the sample (Kasas et al., 1997; Hansma et al., 1999; Thomson et al., 1999; Bonin et al., 2000). To our knowledge, high quality images of small RNA molecules in solution have not been obtained by AFM. Small dsDNA molecules, however, have been imaged (Hansma et al., 1996). In the latter study, single-stranded DNA, as well as 25- and 50-bp dsDNAs, were observed to be globular in shape. The 50-bp DNA samples contained some rod-shaped conformations, proposed to be two colinearly stacked molecules, whereas 100-bp DNA samples appeared rod-like or slightly curved. More recent work has focused on protein–nucleic acid complexes and the topography of large DNA molecules (e.g., Hansma et al., 1992, 1993, 1999; Kasas et al., 1997; Bustamante et al., 1999; Houchens et al., 2000).

Here, we have employed tapping-mode AFM to image single hairpin ribozyme–substrate complexes in an aqueous buffer similar to the one typically used in activity assays, except that 3 mM $NiCl_2$ was added to bind the RNA to the mica surface. The constructs utilized have extended terminal helices to increase visibility by microscopy (Fig. 1C). The same constructs have previously been studied in solution, observing their electric field-induced transient electric dichroism (TED) decays to calculate average interdomain bending angles (Porschke et al., 1999). In the TED study, significant differences in rotational diffusion properties, interpreted as differences in average interdomain bending angles, were detected when comparing constructs with or without a cleavage site mutation G + 1A and a 6-nt insertion, for flexibility at the interdomain junction (Fig. 1C). Here, we describe the optimization of imaging buffer and sample preparation for AFM visualization of individual hairpin ribozyme–substrate complexes in solution. With these conditions, we have acquired images of this small RNA enzyme, and show that it is possible to directly observe structural differences between active and inactive variants.

RESULTS AND DISCUSSION

A prerequisite for obtaining high-quality AFM images of biological samples on muscovite mica in aqueous buffer is the immobilization of the specimen on the mica surface (Wagner, 1998). The simplest and most common immobilization technique is physical adsorption from the solution. However, muscovite mica is a highly hydrophilic, negatively charged aluminosilicate. This property impairs adsorption of negatively charged nucleic acids. As expected, initial trials showed that the hairpin ribozyme did not adsorb to mica in a manner that was adequate for imaging in a standard reaction buffer (12 mM $MgCl_2$ at pH 7.5). However, DNA has been shown to adsorb well in the presence of divalent transition ion metals such as Ni^{2+}, Co^{2+}, or Zn^{2+} (Bustamante et al., 1992; Bezanilla et al., 1995; Hansma & Laney, 1996). We therefore systematically tested such additives in our imaging buffer.

We obtained the best AFM images by preconditioning the mica surface briefly with 1 mM $NiCl_2$, and by adding 3 mM $NiCl_2$ to an imaging buffer composed of 20 mM HEPES-KOH, pH 7.5, 12 mM $MgCl_2$ (see Materials and Methods); all images reported here were obtained in this fashion. Background particles appear in the images (see below) that we found to be an inherent artifact associated with the use of Ni^{2+} for binding RNA to the mica surface. We attempted to eliminate this background by reducing the $NiCl_2$ concentration, but this severely inhibited binding of the RNA to the surface, while not alleviating the background problem (data not shown). Apparently, $Ni(OH)_2$ precipitates on the surface and its presence is coincident with enhanced binding. Consistent with this notion, reducing the pH of the imaging buffer to pH 7.0 eliminated the background, yet also led to a complete loss of RNA binding to the mica (data not shown).

We also tested other metals, such as varying concentrations of $MgCl_2$ (up to 100 mM), $CaCl_2$ and $SrCl_2$ (1–10 mM), and $Co(NH_3)_6Cl_3$ (0.1–2 mM), none of which produced images of the quality observed with 3 mM Ni^{2+}. Co^{2+} was the next best metal, but perhaps due to weak binding, the RNA appeared at low resolution, and tended to be rubbed off the mica surface by the probe. $ZnCl_2$ caused the RNA to appear as large amorphous aggregates, probably resulting from precipitation of $Zn(OH)_2$ around the RNA, yielding unacceptably low image quality (data not shown).

To show biological function of the hairpin ribozyme under AFM conditions, we tested endonucleolytic cleavage activity of our constructs HP2 and HP3 under optimized imaging conditions. Previously, we have shown that the active construct, HP3 (Fig. 1C), cleaves at a rate constant of 0.035 min^{-1} under standard conditions (50 mM Tris-HCl, pH 7.5, 12 mM $MgCl_2$, 25 °C). This rate is approximately threefold slower than our standard hairpin constructs utilized for activity assays. HP2, which carries a detrimental G + 1A mutation at the cleavage site, did not produce cleavage products under these conditions, as expected (Porschke et al., 1999). Here, we were able to confirm these results and extend them to the inclusion of Ni^{2+} in the assays. Figure 2 shows that construct HP2 did not cleave under any conditions, whereas HP3 is active after addition of $MgCl_2$, and the presence of $NiCl_2$ does not inhibit the Mg^{2+}-dependent reaction. The relatively low abundance of cleavage product after 60 min at 37 °C is due

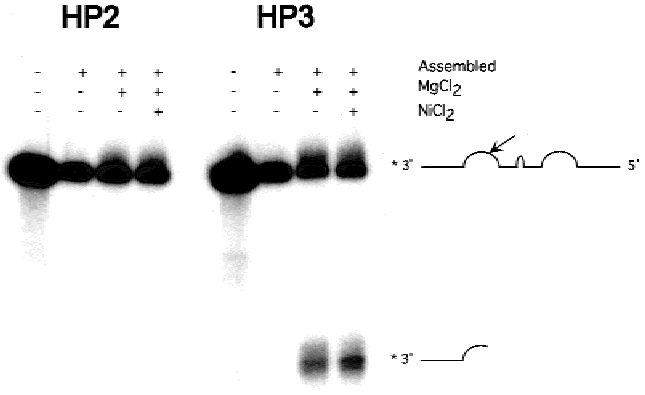

FIGURE 2. Cleavage activity assay of the HP2 and HP3 constructs. The substrate strands were 3′-end labeled with ^{32}pCp and either left untreated or annealed to the 5′ ribozyme segment for the activity assay. Reactions were incubated at 37 °C for 60 min in 20 mM HEPES-KOH, pH 7.5, in the absence or presence of 12 mM Mg^{2+} and 3 mM Ni^{2+}, as indicated. Note that the extent of cleavage in construct HP3 is limited by the fact that cleavage products cannot dissociate; hence the observed extent of cleavage reflects an equilibrium between cleavage and ligation.

to the high propensity of this hairpin ribozyme construct to religate cleavage products that do not dissociate due to extended helix 1. It has been shown that increased binding energy of the products from this reaction shifts equilibrium in favor of ligation (Hegg & Fedor, 1995). We also performed fluorescence resonance energy transfer (FRET) experiments that monitor docking of the two domains (Walter et al., 1998) and found that the addition of Ni^{2+} reduces Mg^{2+}-induced docking in solution to some extent (data not shown); however, this does not inhibit the catalytic activity of the ribozyme.

AFM images of untreated mica in imaging buffer without $NiCl_2$ depict a smooth surface (Fig. 3A). In contrast, AFM scans obtained using standard imaging buffer (20 mM HEPES-KOH, pH 7.5, 12 mM $MgCl_2$, 3 mM $NiCl_2$) without RNA show background particles that accumulate over time, as would be expected for a $Ni(OH)_2$ precipitate. We therefore prepared the imaging buffer fresh for each AFM session to minimize the amount of precipitate. The observed background particles are globular or slightly rodlike in shape (Fig. 3B). Similar particles appear in the AFM images of the hairpin ribozyme constructs, together with a population of larger objects with distinct morphology—the individual RNA molecules. Our analysis of the particle size and the clear difference in appearance between RNA molecules and background particles enabled us to easily distinguish them (Fig. 4). We therefore used $NiCl_2$ as the additive in the imaging buffer.

First, we imaged a linear dsRNA control, 72 bp in length (Fig. 3C). It has the same sequence as hairpin ribozyme construct HP1 (Fig. 1C), except that the in-

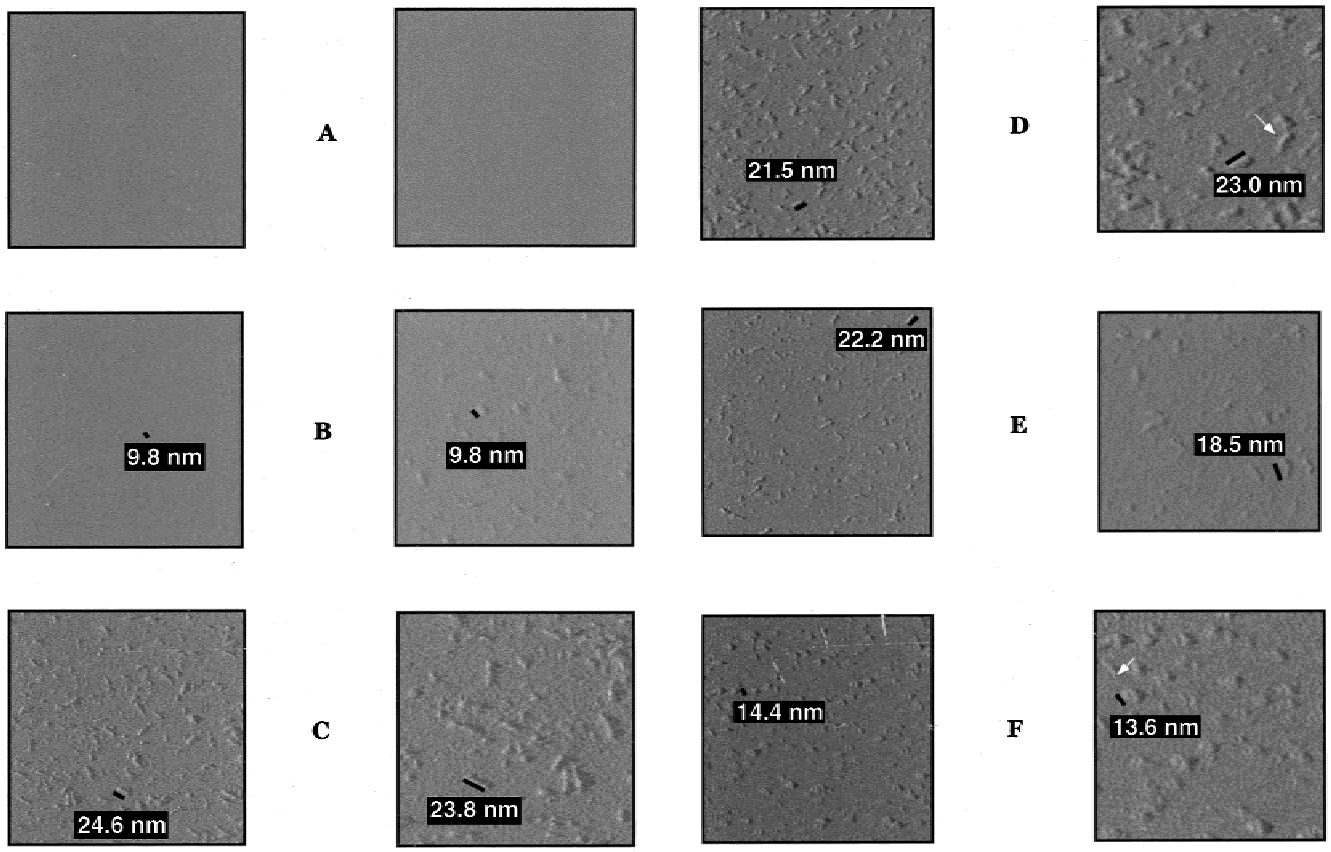

FIGURE 3. AFM images of the hairpin ribozyme in solution. The images are displayed pairwise, with 500 nm × 500 nm overview scans on the left and selected areas of 250 nm × 250 nm magnified on the right. **A**: Freshly cleaved mica, no $NiCl_2$ treatment. Imaging buffer: 20 mM HEPES-KOH, pH 7.5, 12 mM $MgCl_2$. **B**: Freshly cleaved mica, treated with $NiCl_2$. Standard imaging buffer: 20 mM HEPES-KOH, pH 7.5, 12 mM $MgCl_2$, 3 mM $NiCl_2$. **C**: 72-bp dsRNA, imaged under standard conditions (on freshly cleaved and $NiCl_2$ treated mica in 20 mM HEPES-KOH, pH 7.5, 12 mM $MgCl_2$, 3 mM $NiCl_2$). This RNA serves as a control; it shares the 5′ ribozyme segment of HP1 to HP3, but has a fully complementary 3′ segment to make it a rigid rod. **D**: Construct HP1, imaged under standard conditions. This RNA contains loop A (with a G + 1A mutation) and loop B, but no hinge insertion (Fig. 1C). White arrow points out a curved individual. **E**: Construct HP2, imaged under standard conditions. This RNA contains loop A (with a G + 1A mutation) and loop B, and a 6-nt interdomain insertion to create a flexible hinge (Fig. 1C). **F**: Catalytically active construct HP3, imaged under standard conditions. This RNA contains loop A (with the catalytically essential G + 1) and loop B as well as a 6-nt interdomain insertion to create a flexible hinge (Fig. 1C). The structural change that results from the presence of G + 1 is dramatic and emphasizes the importance of this base in tertiary structure formation of the active ribozyme–substrate complex. The white arrow points out an individual molecule in the open conformation.

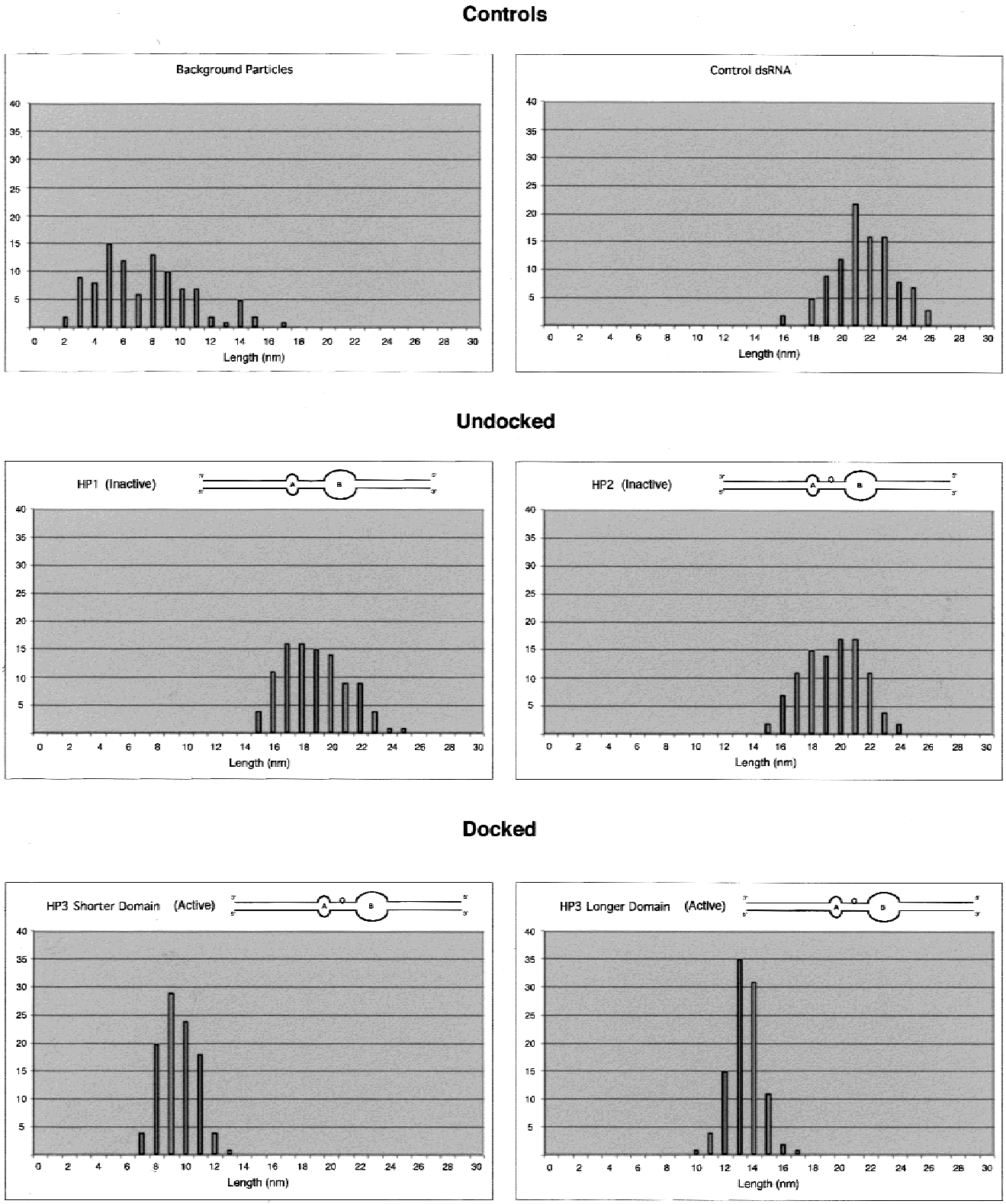

FIGURE 4. Length distributions of all the constructs imaged in Figure 3. Thirty bins were created, one for each nanometer of length. Length measurements were rounded to the nearest integer before being placed in the corresponding bin. For example, a molecule measuring 19.4 nm would be placed in the 19 nm bin. The y axis is number of particles per bin. One hundred particles were measured for each plot.

ternal loop regions are Watson–Crick base paired throughout. With this control RNA, we observed a uniform population of rodlike objects (Fig. 4), clearly distinct from the $Ni(OH)_2$ particles in the background control slide. This length analysis compares favorably with a calculated theoretical length of 20.2 nm for a dsRNA of 72 bp, at a rise per base pair of 2.8 Å (Saenger, 1984).

The dsRNA molecules all have different orientations with respect to the scan direction (horizontal). One will notice, however, that no molecules appear oriented exactly parallel to the scan line. The probe would have to walk the entire length of such a molecule without falling off to generate an image of a complete molecule, somewhat akin to walking along a roadside curb, each footstep being a tap of the probe. If the probe walked, for instance, over only part of the molecule in one pass, an image would be generated of one or more particles (i.e., another part of the molecule might show up on the next or a previous pass) similar to, but shorter than, a full-length molecule. Some background particles in the experimental images may be a result of this effect.

Next, we obtained AFM images of HP1 (Fig. 3D), a catalytically inactive hairpin ribozyme construct with the G + 1A mutation and with a rigid interdomain hinge region (Fig. 1C), changes which lock the ribozyme into an extended conformation. This RNA appears to be slightly shorter than the fully dsRNA control (Fig. 4). This length decrease is consistent with replacement of Watson–Crick base paired regions with nonhelical internal loops. HP2 is a catalytically inactive hairpin ribozyme construct with the G + 1A mutation and with a flexible interdomain hinge region, created by a 6-nt insertion (Fig. 1C). This RNA (Fig. 3E) also appears slightly shorter than the dsRNA control (Fig. 4).

HP3, the catalytically active construct with the cleavage site G + 1 and a flexible hinge to enable the internal loops to interact (Fig. 1C), presents an image that is entirely different from those of all the other constructs (Fig. 3F). In contrast to HP1 and HP2, the molecule does not only partially bend, but displays two dissimilar structures that are aligned side by side. We refer to these as the "shorter domain" and "longer domain" as we can not conclusively determine which is the A or B domain with these data alone. A comparison of the length analyses for each domain indicates a clear difference in length as measured from the hinge (Fig. 4). This appearance is suggestive of the stably docked or closed conformation of the hairpin ribozyme. Of particular interest is the asymmetry of the RNA molecules in these images between domains (Fig. 5). Because the two domains of HP3, as separated by the hinge, are similar in length (the equivalent of 35 and 37 bp for domains A and B, respectively), this observation might suggest a more complicated docking event than a simple collapse around the hinge region. The two domains likely require asymmetric alignment for productive interaction in the docked complex. This is in agreement with asymmetry inferred from gel electrophoresis experiments and FRET analysis of various hairpin ribozyme constructs (Murchie et al., 1998; Zhao et al., 2000).

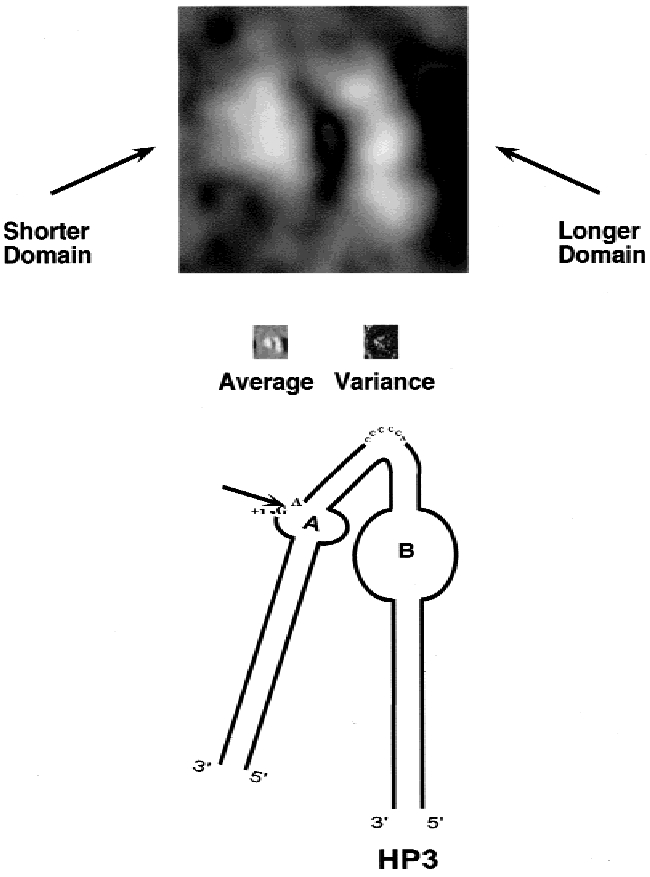

FIGURE 5. Enlarged, contrast-enhanced average image of particles from the active population, HP3. Original average and variance maps show the region with highest variation is the outer fringe of the shorter domain. Comparison with a diagram of what might be expected from symmetric alignment of helices 1 and 4 for docking (Figs. 1C, 3F).

Due to their regularity, the individual active particles were amenable to image processing techniques developed for the electron microscopy field (Frank et al., 1996). In an effort to generate the clearest possible image, we varied which individual particles were chosen as well as the total number of particles that were subjected to the calculations. However, it became apparent that the highest quality processed image was obtained from only six particles. Perhaps this is due to the resolution limits of AFM in tapping mode under fluid. It is conceivable the raw amplitude plots are close enough to the resolution limit of the technology that further improvement by this technique, without better probes to create higher resolution data, for example, is impossible. The resultant average and variance maps are displayed (Fig. 5) alongside an enlarged and contrast-enhanced version of the average active particle, created to ease viewing.

One will also notice objects in our images of HP3 that look like a single rod, similar to those in images of HP1 (see white arrow in Fig. 3F). These molecules appear to reside in a similarly open conformation as HP1 where the two ribozyme domains colinearly stack (Fig. 1C). It is important to note that, under our imaging conditions (20 mM HEPES-KOH, pH 7.5, 12 mM $MgCl_2$, 3 mM $NiCl_2$), cleavage does occur (see Fig. 2). After cleavage, the long binding arms of the 5′ and 3′ products are expected to prevent the ribozyme–product complex from dissociation (Hegg & Fedor, 1995; data not shown). Thus, the ribozyme is in equilibrium between cleavage and ligation. The HP3 sample therefore will contain some cleaved and some intact complexes, both of which form open and closed conformers. However, we have shown that cleavage changes neither the equilibrium position between nor the structures of the open and closed conformers (Walter et al., 1999). Hence, although there will be four different molecular species present—with either cleaved or intact substrate strand in either the open or closed conformation—we can expect to structurally distinguish only open and closed conformers, consistent with our observations by AFM. From TED experiments, we previously inferred an average interdomain bending angle of 80 ± 20° for HP3, consistent with the heterogeneous population of strongly bent (docked) and straight (extended) conformers imaged by AFM.

In summary, we were able to produce AFM images of individual hairpin ribozymes differing in their ability to form the active docked conformation. The observed shapes and contour lengths are largely consistent with previous bulk-solution measurements of the TED decays of the same RNA constructs. From these, we were able to generate a higher quality image of an averaged active particle. In our experiments, the active docked construct HP3 appears in our AFM images as an asymmetrically docked conformation with one domain clearly shorter than the other domain. This observation appears to be an indication of a more complex tertiary structure than would be expected from simple alignment of domains A and B. From the variance map presented in Figure 5, it is clear that the shorter domain is most variable on the outer fringes. An early three-dimensional model obtained by computer modeling presented the docked ribozyme–substrate complex as fairly symmetric. The two domains were modeled to come together as two side-by-side helices (Earnshaw et al., 1997). Recent results from our laboratory provide strong evidence for a sharp bend within domain A of the hairpin ribozyme (R. Pinard, D. Lambert, J. Heckman, J. Esteban, C. Gundlach, K. Hampel, G. Glick, N. Walter, F. Major, and J. Burke, unpubl.). A possible explanation for our shorter domain and its variability in the images of the active construct is the extended helix one being forced off the mica by an internal kink.

MATERIALS AND METHODS

Preparation of RNA samples

T7 RNA polymerase was used to transcribe partially double-stranded DNA templates to obtain the 5′ and 3′ strand of each ribozyme construct, essentially as described (Milligan & Uhlenbeck, 1989), but using 7.5 mM of each NTP and pyrophosphatase for higher yields (Cunningham & Ofengand, 1990). After 4 h at 37 °C, the reactions were phenol extracted, the RNA was ethanol precipitated, and then purified by 20% denaturing, 8 M urea, polyacrylamide gel electrophoresis. RNA transcripts were recovered by cutting out the major product band as visualized by its UV shadow followed by diffusion elution from the gel slices. The eluate was chloroform extracted and the RNA was recovered by precipitation with ethanol.

The two strands of each ribozyme construct were annealed at a concentration of 20 μM in HE buffer (10 mM HEPES-KOH, pH 7.5, 0.1 mM EDTA) by thermal denaturation (2 min, 90 °C) followed by slow cooling to 22 °C. Nondenaturing loading buffer was added to a final concentration of 6% glycerol and 0.01% bromophenol blue. The annealed RNA was then directly applied to a 10% nondenaturing polyacrylamide gel in 1 × TBE buffer for purification. Bands were visualized by their UV shadow, cut from the gel, and eluted overnight at 4 °C in HE buffer. The recovered annealed RNA was concentrated and washed three times with 2 mL HE buffer by ultrafiltration through a Centricon 10 filter (Millipore). Finally, the RNA was diluted to 100 nM (~5 ng/μL) in HE buffer and stored in aliquots at −20 °C. To confirm homogeneity, the annealed RNA was 5′-^{32}P labeled with T4 polynucleotide kinase and analyzed on a 10% nondenaturing polyacrylamide gel.

AFM imaging

The microscope used was a BioScope Nanoscope IIIa (Digital Instruments, Santa Barbara, California) supported by an air-cushioned table. Oxide-sharpened silicon nitride probes were obtained from Advanced Surface Microscopy (Indianapolis, Indiana). We employed the 100-μm probes, with a spring constant of 0.38 N/m. Samples were prepared for imaging on a freshly cleaved muscovite mica substrate previously mounted on a glass coverslip. After optimal buffer composition and sample concentration were identified (10 nM RNA was typically best—concentrations above 100 nM result in apparent aggregation or precipitation on the mica), the limiting factor for high-resolution data was found to be the probe (Taatjes et al., 1999). Consequently, during any given imaging session, if image quality was low, the probe was discarded and a new one mounted.

The mica surface was preconditioned with 10 μL of 1 mM $NiCl_2$ for 1 min, rinsed three times with 100 μL of sterile deionized water, and blown dry with compressed air. Ten microliters of 1–100 nM RNA sample was applied to the treated mica, followed immediately by 150 μL imaging buffer (20 mM HEPES-KOH, pH 7.5, 12 mM $MgCl_2$, 3 mM $NiCl_2$). At this point, the prepared sample was mounted on the microscope for data collection. The preparations were typically used for 1–2 h before background particles started to accumulate and a fresh sample was required.

In general, 500 nm or 1 μm square scans were performed using tapping mode in fluid, at a scan rate of 2.105 Hz, 512 samples and a setpoint of approximately 0.3 V (varied). The only manipulation of the resultant plots was zooming in on particular molecules or areas for emphasis and/or measurements (Nanoscope IIIa, software version 4.23b7). Contour length measurements were performed by drawing a traverse line alongside the molecule on the monitor, utilizing the amplitude plot. Results are discussed as mean $\pm$ SD.

Activity assay

Transcripts of the substrate strands of HP2 and HP3 were 3′-end-labeled with ^{32}pCp using T4 RNA ligase. The labeled transcripts were gel purified by 15% denaturing, 8 M urea, polyacrylamide gel electrophoresis. Bands were visualized by autoradiography, cut out, and the RNA eluted by diffusion from the gel slices. The transcripts were recovered following chloroform extraction by ethanol precipitation.

Trace amounts of the ^{32}P-labeled (50,000 cpm per reaction), combined with unlabeled, substrate strand was annealed to the substrate-binding strand for a final concentration of 100 nM annealed RNA, by heating to 90 °C for 2 min and slow cooling to room temperature in HE buffer, as described above. The annealed mixture was then diluted 1:15 in HE, HM, or HMN buffer (20 mM HEPES, pH 7.5, plus 0.1 mM Na_2EDTA, or 12 mM $MgCl_2$, or 12 mM $MgCl_2$/3 mM $NiCl_2$, respectively) in a 15-μL reaction volume. The reactions were incubated at 37 °C for 60 min. Reaction products were separated using 15% denaturing, 8 M urea, polyacrylamide gels and visualized by autoradiography.

Image processing

The SPIDER WEB image processing package (Frank et al., 1996) was utilized to obtain an averaged image of the active construct and the corresponding variance map. WEB, the graphical interface, was used to pick particles from the amplitude plots of previously acquired AFM images. Subsequently, these particles were aligned by the RT SQ subprogram according to xy shift and angle of rotation parameters obtained from the AP SR subprogram. Average and variance maps were calculated with the AS R subprogram performed on the aligned particles. The average map was enlarged and contrast enhanced with Adobe Photoshop. Original average and variance maps are also displayed.

ACKNOWLEDGMENTS

We would like to thank Dr. Douglas Taatjes and Anthony S. Quinn of the University of Vermont Cell Imaging Facility for helpful discussions and technical assistance as well as Dr. Jie Yang for encouragement at the onset of this project.

Received December 11, 2000; returned for revision January 3, 2001; revised manuscript received March 6, 2001

REFERENCES

Bezanilla M, Manne S, Laney DE, Lyubchenko YI, Hansma HG. 1995. Adsorption of DNA to mica, silylated mica and minerals: Characterization by atomic force microscopy. *Langmuir 11*:655–659.

Bonin M, Oberstrass J, Lukacs N, Ewert K, Oesterschulze E, Kassing R, Nellen W. 2000. Determination of preferential binding sites for anti-dsRNA antibodies on double-stranded RNA by scanning force microscopy. *RNA 6*:563–570.

Bustamante C, Guthold M, Zhu X, Yang G. 1999. Facilitated target location on DNA by individual *Escherichia coli* RNA polymerase molecules observed with the scanning force microscope operating in liquid. *J Biol Chem 274*:16665–16668.

Bustamante C, Rivetti C, Keller DJ. 1997. Scanning force microscopy under aqueous solutions. *Curr Opin Struct Biol 7*:709–716.

Bustamante C, Vesenka J, Tang CL, Rees W, Guthold M, Keller R. 1992. Circular DNA molecules imaged in air by scanning force microscopy. *Biochemistry 31*:22–26.

Butcher SE, Allain FH-T, Feigon J. 1999. Solution structure of the loop B domain from the hairpin ribozyme. *Nat Struct Biol 6*:212–216.

Butcher SE, Heckman JE, Burke JM. 1995. Reconstitution of hairpin ribozyme activity following separation of functional domains. *J Biol Chem 270*:29648–29651.

Buzayan JM, Hampel A, Bruening G. 1986. Nucleotide sequence and newly formed phosphodiester bond of spontaneously ligated satellite tobacco ringspot virus RNA. *Nucleic Acids Res 14*: 9729–9743.

Cai Z, Tinoco I Jr. 1996. Solution structure of loop A from the hairpin ribozyme from tobacco ringspot virus satellite. *Biochemistry 35*:6026–6036.

Cunningham PR, Ofengand J. 1990. Use of inorganic pyrophosphatase to improve the yield of in vitro transcription reactions catalyzed by T7 RNA polymerase. *Biotechniques 9*:713–714.

Drygin YF, Bordunova OA, Gallyamov MO, Yaminsky IV. 1998. Atomic force microscopy examination of tobacco mosaic virus and virion RNA. *FEBS Lett 425*:217–221.

Earnshaw DJ, Masquida B, Muller S, Sigurdsson ST, Eckstein F, Westhof E, Gait MJ. 1997. Inter-domain cross-linking and molecular modelling of the hairpin ribozyme. *J Mol Biol 274*:197–212.

Engel A, Lyubchenko Y, Muller D. 1999. Atomic force microscopy: A powerful tool to observe biomolecules at work. *Trends Cell Biol 9*:77–80.

Feldstein PA, Bruening G. 1993. Catalytically active geometry in the reversible circularization of 'mini-monomer' RNAs derived from the complementary strand of tobacco ringspot virus satellite RNA. *Nucleic Acids Res 21*:1991–1998.

Frank J, Radermacher M, Penczek P, Zhu J, Li Y, Ladjadj M, Leith A. 1996. SPIDER and WEB: Processing and visualization of images in 3D electron microscopy and related fields. *J Struct Biol 116*:190–199.

Fritz J, Anselmetti D, Jarchow J, Fernandez-Busquets X. 1997. Probing single biomolecules with atomic force microscopy. *J Struct Biol 119*:165–171.

Hampel A, Tritz R. 1989. RNA catalytic properties of the minimum (−)sTRSV sequence. *Biochemistry 28*:4929–4933.

Hampel KJ, Walter NG, Burke JM. 1998. The solvent-protected core of the hairpin ribozyme–substrate complex. *Biochemistry 37*: 14672–14682.

Hansma HG, Bezanilla M, Zenhausern F, Adrian M, Sinsheimer RL. 1993. Atomic force microscopy of DNA in aqueous solutions. *Nucleic Acids Res 21*:505–512.

Hansma HG, Golan R, Hsieh W, Daubendiek SL, Kool ET. 1999. Polymerase activities and RNA structures in the atomic force microscope. *J Struct Biol 127*:240–247.

Hansma HG, Hoh JH. 1994. Biomolecular imaging with the atomic force microscope. *Annu Rev Biophys Biomol Struct 23*:115–139.

Hansma HG, Kim KJ, Laney DE, Garcia RA, Argaman M, Allen MJ, Parsons SM. 1997. Properties of biomolecules measured from atomic force microscope images: A review. *J Struct Biol 119*: 99–108.

Hansma HG, Laney DE. 1996. DNA binding to mica correlates with cationic radius: Assay by atomic force microscopy. *Biophys J 70*: 1933–1939.

Hansma HG, Pietrasanta L. 1998. Atomic force microscopy and other scanning probe microscopies. *Curr Opin Chem Biol 2*:579–584.

Hansma HG, Revenko I, Kim K, Laney DE. 1996. Atomic force microscopy of long and short double-stranded, single-stranded and triple-stranded nucleic acids. *Nucleic Acids Res 24*:713–720.

Hansma HG, Sinsheimer RL, Li MQ, Hansma PK. 1992. Atomic force microscopy of single- and double-stranded DNA. *Nucleic Acids Res 20*:3585–3590.

Hegg LA, Fedor MJ. 1995. Kinetics and thermodynamics of intermolecular catalysis by hairpin ribozymes. *Biochemistry 34*: 15813–15828.

Heinz WF, Hoh JH. 1999. Spatially resolved force spectroscopy of biological surfaces using the atomic force microscope. *Trends Biotechnol 17*:143–150.

Houchens CR, Montigny W, Zeltser L, Dailey L, Gilbert JM, Heintz NH. 2000. The dhfr oribeta-binding protein RIP60 contains 15 zinc fingers: DNA binding and looping by the central three fingers and an associated proline-rich region. *Nucleic Acids Res 28*:570–581.

Kasas S, Thomson NH, Smith BL, Hansma HG, Zhu X, Guthold M, Bustamante C, Kool ET, Kashlev M, Hansma PK. 1997. *Escherichia coli* RNA polymerase activity observed using atomic force microscopy. *Biochemistry 36*:461–468.

Komatsu Y, Kanzaki I, Ohtsuka E. 1996. Enhanced folding of hairpin ribozymes with replaced domains. *Biochemistry 35*:9815–9820.

Lindsay SM. 1994. Biological scanning probe microscopy comes of age. *Biophys J 67*:2134–2135.

Lyubchenko YL, Jacobs BL, Lindsay SM. 1992. Atomic force microscopy of reovirus dsRNA: A routine technique for length measurements. *Nucleic Acids Res 20*:3983–3986.

Miles M. 1997. Scanning probe microscopy. Probing the future. *Science 277*:1845–1847.

Milligan JF, Uhlenbeck OC. 1989. Synthesis of small RNAs using T7 RNA polymerase. *Methods Enzymol 180*:51–62.

Murchie AI, Thomson JB, Walter F, Lilley DM. 1998. Folding of the hairpin ribozyme in its natural conformation achieves close physical proximity of the loops. *Mol Cell 1*:873–881.

Pinard R, Lambert D, Walter NG, Heckman JE, Major F, Burke JM. 1999. Structural basis for the guanosine requirement of the hairpin ribozyme. *Biochemistry 38*:16035–16039.

Porschke D, Burke JM, Walter NG. 1999. Global structure and flexibility of hairpin ribozymes with extended terminal helices. *J Mol Biol 289*:799–813.

Saenger W. 1984. *Principles of nucleic acid structure*. New York: Springer-Verlag.

Taatjes DJ, Quinn AS, Lewis MR, Bovill EG. 1999. Quality assessment of atomic force microscopy probes by scanning electron microscopy: Correlation of tip structure with rendered images. *Microsc Res Tech 44*:312–326.

Thomson NH, Smith BL, Almqvist N, Schmitt L, Kashlev M, Kool ET, Hansma PK. 1999. Oriented, active *Escherichia coli* RNA polymerase: An atomic force microscope study. *Biophys J 76*: 1024–1033.

Wagner P. 1998. Immobilization strategies for biological scanning probe microscopy. *FEBS Lett 430*:112–115.

Walter NG, Burke JM. 1998. The hairpin ribozyme: Structure, assembly and catalysis. *Curr Opin Chem Biol 2*:303.

Walter NG, Burke JM, Millar DP. 1999. Stability of hairpin ribozyme tertiary structure is governed by the interdomain junction. *Nat Struct Biol 6*:544–549.

Walter NG, Hampel KJ, Brown KM, Burke JM. 1998. Tertiary structure formation in the hairpin ribozyme monitored by fluorescence resonance energy transfer. *EMBO J 17*:2378–2391.

Yang J, Shao Z. 1995. Recent advances in biological atomic force microscopy. *Micron 26*:35–49.

Zhao ZY, Wilson TJ, Maxwell K, Lilley DM. 2000. The folding of the hairpin ribozyme: Dependence on the loops and the junction. *RNA 6*:1833–1846.